mater.scichina.com link.springer.com
Published online 31 January 2018 | https://doi.org/10.1007/s40843-017-9215-3
Sci China Mater 2018, 61(8): 1049–1056

In-situ growth of ultrathin MoS_2 nanosheets on sponge-like carbon nanospheres for lithium-ion batteries

Ling Chen, Hao Jiang*, Yanjie Hu, Haiyan Wang and Chunzhong Li*

ABSTRACT **Developing novel electrode materials for lithium-ion batteries (LIBs) with rapid charge/discharge capability and high cycling stability remains a big challenge to date. Herein, we demonstrate the design and synthesis of ultrathin MoS_2 nanosheets *in-situ* grown on sponge-like carbon nanospheres by a simple diffusion-controlled process. The unique sponge-like carbon nanosphere core can be used as "reservoir" of electrolyte by adsorbing to shorten the ion-diffusion path, and meanwhile as "elastomer" to alleviate the structural change of the MoS_2 nanosheets during the charge/discharge processes. Furthermore, the vertical ultrathin MoS_2 nanosheets with broadened interlayer space greatly enrich the electrochemical active sites. Consequently, the as-obtained MoS_2/C nanospheres exhibit increased specific capacities at various rates with superior cycling stability compared to the MoS_2/C floccules. It is reckoned that the present concept can be extended to other electrode materials for achieving high-rate and stable LIBs.**

Keywords: MoS_2, sponge-like carbon, nanosphere, high-rate, lithium-ion batteries

INTRODUCTION

Two-dimensional (2D) nanomaterials have received considerable attention in the fields of energy, catalysis, sensor, and so forth in view of their intriguing properties caused by the single-atom-thick [1–5]. The family of 2D nanomaterials include graphene, transition metal dichalcogenides, black phosphorus and MXenes, etc. Among them, molybdenum disulfide (MoS_2) has been proved to be a promising anode material for lithium ion batteries (LIBs) due to their larger interlayer space (0.62 nm> 0.34 nm for the commercial graphite anode) and higher lithium storage capacity (669 mA h g^{-1}>372 mA h g^{-1} for graphite) [6–10]. However, the low conductivity and structural change during charge/discharge processes inevitably give rise to the rapid capacity fading. Furthermore, just like other 2D nanomaterials, the easy stacking/restacking behavior makes it difficult to infiltrate electrolyte, causing a long ion transfer path. Therefore, solving these issues will promote the practical application of MoS_2-based anode materials for high-performance LIBs.

Hollow nanostructures have always been a hot topic in energy-related fields because of their large specific surface area, big interior void space and diversified building blocks [11–14]. For example, Lou *et al.* realized the controllable synthesis of various hollow nanostructured materials, such as VO_2 hollow nanospheres [15], SnO_2 hollow nanoboxes [16] and α-Fe_2O_3 hollow nanotubes [17]. Wang *et al.* also developed many hollow nanospheres with multi-layered shell including Co_3O_4 [18], α-Fe_2O_3 [19], etc. Such hollow nanostructures can not only enrich electrochemical reaction active sites but also effectively shorten the diffusion path of ions, significantly improving their specific capacity. Nevertheless, the inherent low conductivity still exists. The pivotal to addressing this issue is to rationally hybridize with high conductive carbon, popularly loading 2D nanosheets on various carbon substrate [20–22], such as ultrathin MoS_2 nanosheets supported on N-doped hollow carbon nanobox [23], MnO_2 nanosheets distributed on hollow carbon nanospheres [24]. An extensive cycling will unavoidably cause the structural pulverization although these hybrids exhibit high specific capacity because the thin carbon layer microsubstrate is difficult to afford the repeated structural change after a long charge/discharge process. Therefore, it remains a great challenge to simultaneously achieve rapid charge/discharge capability and highly

Key Laboratory for Ultrafine Materials of Ministry of Education, School of Materials Science and Engineering, East China University of Science & Technology, Shanghai 200237, China
* Corresponding authors (emails: jianghao@ecust.edu.cn (Jiang H); czli@ecust.edu.cn (Li C))

structural integrity before and after cycling by designing novel electrode materials for LIBs.

Inspired by the sponge with interconnected porous structure and strong capability to storage liquid, herein, we demonstrate the design and synthesis of ultrathin MoS_2 nanosheets *in-situ* grown on sponge-like carbon nanospheres by a simple diffusion-controlled process. The ultrathin MoS_2 nanosheets with enlarged interlayer distance from 0.62 to 0.89 nm provide abundant electrochemical active sites. The vertical growth on carbon can also accelerate electrons transfer rate. More impressively, the sponge-like carbon nanosphere core can be used as "reservoir" of electrolyte to shorten the ions-diffusion path, and meanwhile as "elastomer" to alleviate the volume change during the charge/discharge processes. As predicted, the as-obtained MoS_2/C nanospheres deliver an increased reversible capacity with superior cycling stability compared with the MoS_2/C floccules. The present idea can be extended to other electrode materials for achieving high-rate and stable LIBs.

EXPERIMENTAL SECTION

Synthesis of the PMo_{12}-PDA precursor

All chemicals were purchased and used without further purification. Typically, 1.1 g of phosphomolybdic acid (PMo_{12}) were dissolved in 100 mL distilled water, forming a yellow solution. After 10 min, 0.1 g of dopamine (DA) were added into the beaker. The mixture was kept stirring for 20 h at room temperature. The solid products from the solution were collected by vacuum filtration and washed with distilled water for 3 times, then dried in the oven at 60°C for 6 h. Finally, the phosphomolybdic acid-polydopamine (PMo_{12}-PDA) solid nanospeheres are obtained.

Synthesis of the MoO_2/C and MoS_2/C nanospheres

The MoO_2/C nanospheres were obtained by calcining the PMo_{12}-PDA precursor at 700°C for 2 h in Ar atmosphere. The MoS_2/C nanospheres were obtained by a further sulfidation. Typically, 30 mg of MoO_2/C hybrids were put into 80 mL of the solvent of ethanol/H_2O (v/v = 3:1). Subsequently, 200 mg of thiourea were added into the above mixture. After being stirred for 15 min, the solution was transferred into a 100 mL Teflon-lined stainless steel autoclave. The autoclave was kept at 200°C for 24 h. The black precipitates were collected by vacuum filtration and washed with distilled water and ethanol for several times, then dried at 60°C for 6 h.

Characterization

The crystallographic phases and morphology of as-obtained products were examined by X-ray diffraction (XRD, Rigaku D/Max 2500 Cu Kα radiation), scanning electron microscopy (SEM, Hitachi, S-4800) and transmission electron microscopy (TEM, JEOL, JEM-2100) with an X-ray energy dispersive spectrometer (EDS) at an accelerating voltage of 200 kV. The characteristic peaks of carbon were analyzed by NEXUS 670 FT-IR Raman spectrometer. Thermogravimetric analysis (NETZSCH STA409PC) was carried out from room temperature to 800°C with a heating rate of 10°C min^{-1} under flowing air.

Electrochemical measurements

Electrochemical measurements were performed on the basis of coin-type 2016 cells. The working electrode was prepared by mixing the as-prepared active materials, carbon black, and poly(vinyl difluoride) (PVDF) at a weight ratio of 7:2:1, and then pasted on pure Cu foil. The coating thickness of materials is about 50 μm. Pure lithium foil was used as the counter electrode, and the separator was a polypropylene membrane (Celgard 2400). The electrolyte consists of a solution of 1 mol L^{-1} $LiPF_6$ in ethylene carbonate (EC)/dimethyl carbonate (DMC) (1:1 in volume). The cells were assembled in an argon-filled glove box. The charge and discharge measurements were carried out on a LAND-CT2001C test system at different current densities. Cyclic voltammogram experiments were performed on an Autolab PGSTAT302N electrochemical workstation at various scan rates.

RESULTS AND DISCUSSION

As illustrated in Fig. 1, the MoS_2/C nanospheres have been synthesized by a simple diffusion-controlled process. The strong oxidant PMo_{12} is a typical anionic molecular metal-oxygen clusters, which can initiate the polymerization of dopamine, forming uniform solid PMo_{12}-PDA nanospheres with a diameter of ~400 nm (Fig. S1). After calcinated at 700°C in Ar atmosphere, the intermediate MoO_2/C nanospheres are obtained. The XRD diffraction peaks in Fig. S2 are mainly indexed to monoclinic MoO_2 phase (JCPDS card No. 65-5787) [25]. The corresponding TEM image shows that the diameter of MoO_2/C nanosphere is ~360 nm. Finally, the MoS_2/C nanospheres are prepared just by a simple sulfidation process, where the ultrathin MoS_2 nanosheets are well-archored on the surface of porous carbon nanospheres. It is noted that the carbonization step is the key to realizing the synthesis of the target products. Without such a

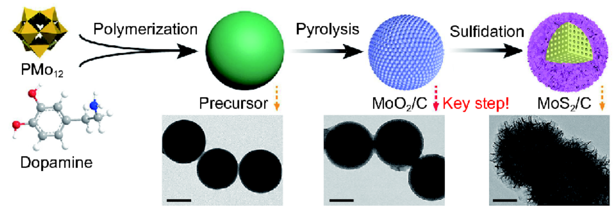

Figure 1 Schematic illustration of the synthesis of MoS_2/C nanospheres and the corresponding TEM images of each stage product. Scale bars are 200 nm.

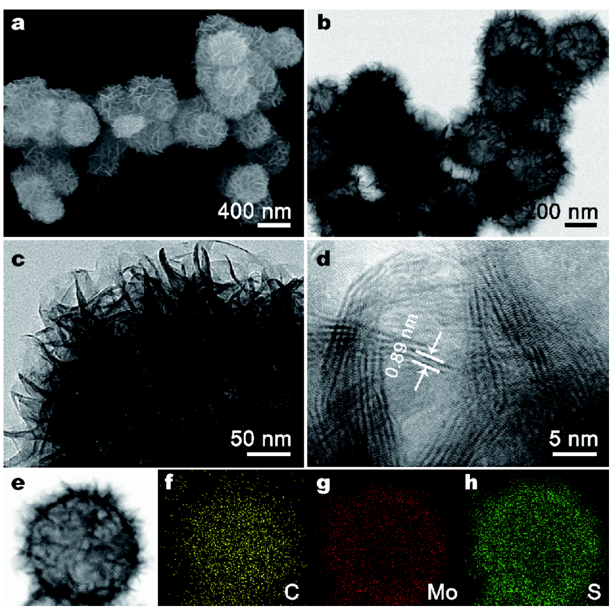

Figure 2 (a) Low-magnification SEM image, (b) low- and (c) high-magnification TEM images, (d) high-resolution TEM image, (e–h) TEM-EDS mapping of the MoS_2/C nanospheres.

treatment, the MoS_2/C floccules (Fig. S3) are used as a control sample for comparing their electrochemical performance with our MoS_2/C nanospheres.

Fig. 2a shows the typical SEM image of the MoS_2/C nanospheres. It can be observed that the uniform flower-like nanospheres (~460 nm) are assembled from amounts of nanosheets. The nanostructure of the products has been further investigated in detail by TEM observation. As shown in Fig. 2b, the interior part of the MoS_2/C nanospheres is almost transparent. The magnified TEM image (Fig. 2c) reveals that the nanosheets are interlocked together, creating abundant pores. The high-resolution TEM image of the products in Fig. 2d gives about 5–10 layered MoS_2 nanosheets with an enlarged interlayer spacing of 0.89 nm, which is larger than that of the normal MoS_2 nanosheets (0.62 nm). Interestingly, the elemental mapping images (Fig. 2e–f) of a representative MoS_2/C nanosphere show that Mo and S are distributed uniformly around the surface of the whole nanosphere while C is mainly dispersed in the inner core with a relatively smaller area. This result suggests that the inner core is composed of carbon. Therefore, the ultrathin MoS_2 nanosheets are assembled on the surface of the carbon nanosphere.

Fig. 3a shows the XRD pattern of the MoS_2/C nanospheres. The diffraction peak at 9.9° is attributed to the interlayer spacing of MoS_2 along the *c*-axis (~0.89 nm) [26,27], consistent with the high-resolution TEM result. An additional peak at 18.3° is also observed, which can be ascribed to the spacing between MoS_2 layer and the carbon layer [28]. The carbon content in the MoS_2/C nanospheres and MoS_2/C floccules is estimated to be 20 and 33.3 wt% according to the thermogravimetric analysis (TGA) (Fig. S4). Raman analysis in Fig. 3b shows two obvious peaks at 1,320 cm^{-1} (D band) and 1,590 cm^{-1} (G band) with I_D/I_G ratio of ~1.62, implying rich defects in the carbon component. Besides, the X-ray photoelectron spectroscopy (XPS) was performed to investigate the chemical states of Mo and S in the hybrids. The peaks at 232.4 and 228.2 eV in Fig. 3c belong to Mo $3d_{3/2}$ and Mo $3d_{5/2}$, which suggest Mo^{4+} in the MoS_2. The presence of another Mo 3d weak peak at ~ 236.0 eV is indexed to Mo^{6+} of MoO_3, resulting from the surface oxidation of the MoS_2/C in air [29]. In S 2p spectrum (Fig. 3d), two peaks at 162.7 eV and 161.8 eV are characteristic peaks of S^{2-} in MoS_2 [30].

The morphology evolution during the sulfidation process is studied to analyze the formation process of the MoS_2/C nanospheres. As shown in Fig. 4a, when the reaction proceeds for ~4 h, the nanosheets begin to appear on the surface of the nanospheres. With reaction time increasing (Fig. 4b–c), the colour of internal nanospheres is gradually getting lighter and the external MoS_2 nanosheets are getting thicker and denser. When reaction time increases to 24 h (Fig. 4d), the final products are obtained with MoS_2 nanosheets vertically grown on the carbon nanospheres. Based on the time-dependent morphology evolution, the whole formation process can be divided into the following steps (Fig. 4e). Initially, the S^{2-} ions released from thiourea react with Mo^{4+} from MoO_2/C nanospheres on the surface, forming thin MoS_2 nanosheets. These MoS_2 nanosheets act as physical barriers, which will hinder the further inward diffusion of S^{2-} ions. With the increase of reaction time, more Mo^{4+} ions diffuse to the surface and then react with S^{2-} ions, leading to the sustained growth of MoS_2 nanosheets. Finally, the

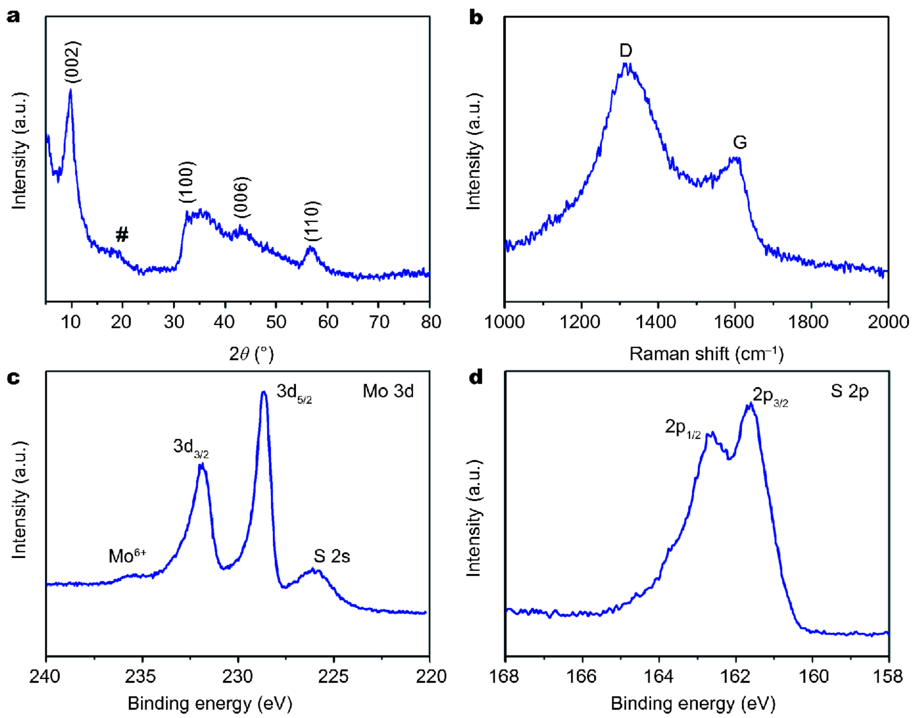

Figure 3 (a) XRD pattern, (b) Raman spectrum and (c, d) XPS spectra of Mo 3d and S 2p of the MoS_2/C nanospheres.

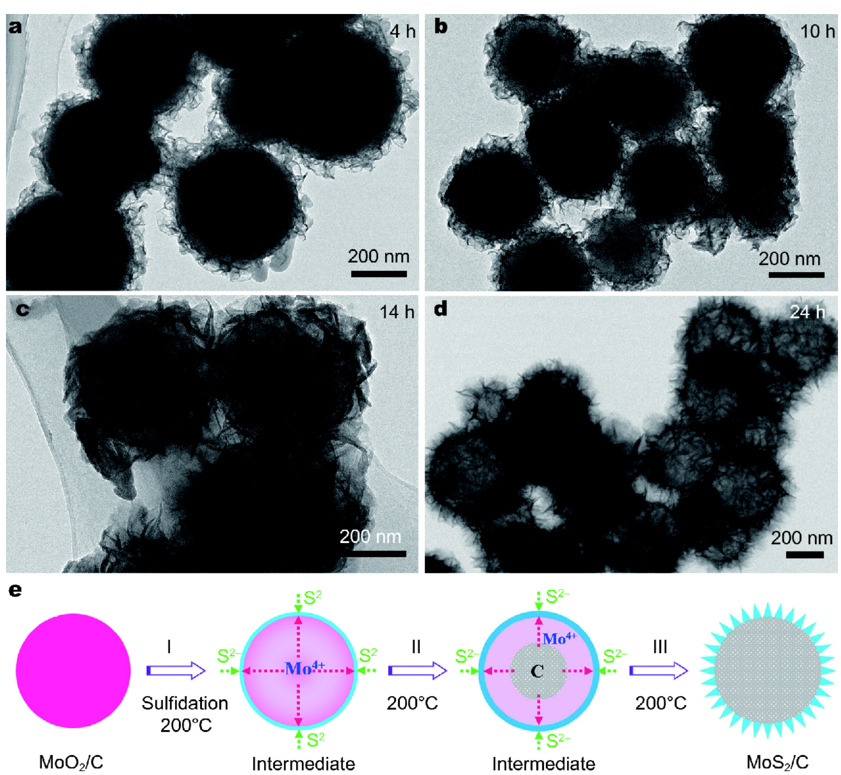

Figure 4 TEM images of products with different sulfidation time: (a) 4 h, (b) 10 h, (c) 14 h, (d) 24 h, and (e) the schematic illustration for the formation of the MoS_2/C nanospheres.

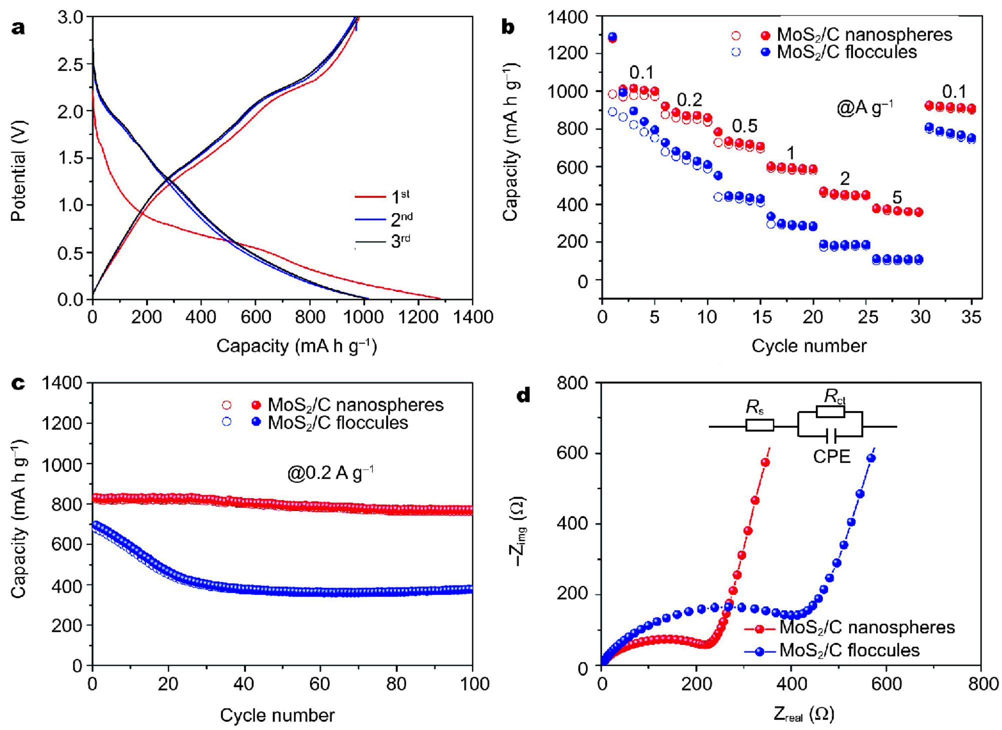

Figure 5 (a) The initial three charge/discharge curves of the MoS_2/C nanospheres at 0.1 A g^{-1}, (b) rate capacity, (c) cycling performance at 0.2 A g^{-1}, and (d) electrochemical impedance spectra of the MoS_2/C nanospheres and MoS_2/C floccules.

MoS_2/C nanospheres are obtained.

The MoS_2/C nanospheres were evaluated as anode materials for lithium ion batteries. Fig. 5a shows the typical charge/discharge curves of MoS_2/C nanospheres in 0.01–3.0 V *vs.* Li/Li^+ at a current density of 0.1 A g^{-1}. The initial discharge and charge capacities are 1,279 and 984 mA h g^{-1} with a Coulombic efficiency (CE) of 76.9%. The capacity loss may result from the formation of solid electrolyte interphase (SEI) and decomposition of electrolyte. The CE increases above 95% in the second cycle with a high reversible capacity of 970 mA h g^{-1}. Fig. 5b shows the rate performance of MoS_2/C nanospheres. The average specific capacities are approximately 970, 850, 710, 585, 444 and 370 mA h g^{-1} at current densities of 0.1, 0.2, 0.5, 1, 2, 5 A g^{-1}, respectively. When the current density returns back to 0.1 A g^{-1}, the specific capacity of MoS_2/C nanospheres can be recovered to 920 mA h g^{-1}, implying a high reversibility. As a comparison, the rate capability of MoS_2/C floccules was also tested, which shows much inferior capacity retention at various current densities. The cycling performance was carried out at a current density of 0.2 A g^{-1} after the rate test. As shown in Fig. 5c, no obvious decay can be observed even after 100 cycles for MoS_2/C nano-spheres, while the MoS_2/C floccules show fast capacity fading. Only a specific capacity of ~320 mA h g^{-1} can be retained. The electrochemical impendence spectra (EIS) of the MoS_2/C nanospheres and the MoS_2/C floccules before cycling are provided in Fig. 5d. The charge transfer resistance (R_{ct}) of MoS_2/C nanospheres is ~223 Ω, which is significantly smaller than that of the MoS_2/C floccules (~549 Ω), thus achieving a rapid charge/discharge capability.

To further study the reaction kinetics of the two hybrids in LIBs, CV tests at different scan rates were carried out. As shown in Fig. 6a and b, the shape of the MoS_2/C nanospheres remains almost unchanged when the scan rates increase from 0.2 to 1 mV s^{-1}, indicating a fast Li^+ insertion and extraction kinetics. The relationship between the sweep rate (v) and peak current (i) obeys a power law: $i=av^b$, where a and b are adjustable parameters. The b-value can be calculated by the slope of the log(v)-log(i) plots. When b = 1, it is a representative non-Faradaic capacitive behavior. When b = 0.5, the electrochemical reaction is a diffusion-controlled process [31,32]. From Fig. 6c and d, the calculated b-values of the MoS_2/C nanospheres are 0.98 for the reduction processes and 0.89 for the oxidation processes, which is much higher than that of the MoS_2/C floccules (b = 0.51 for the

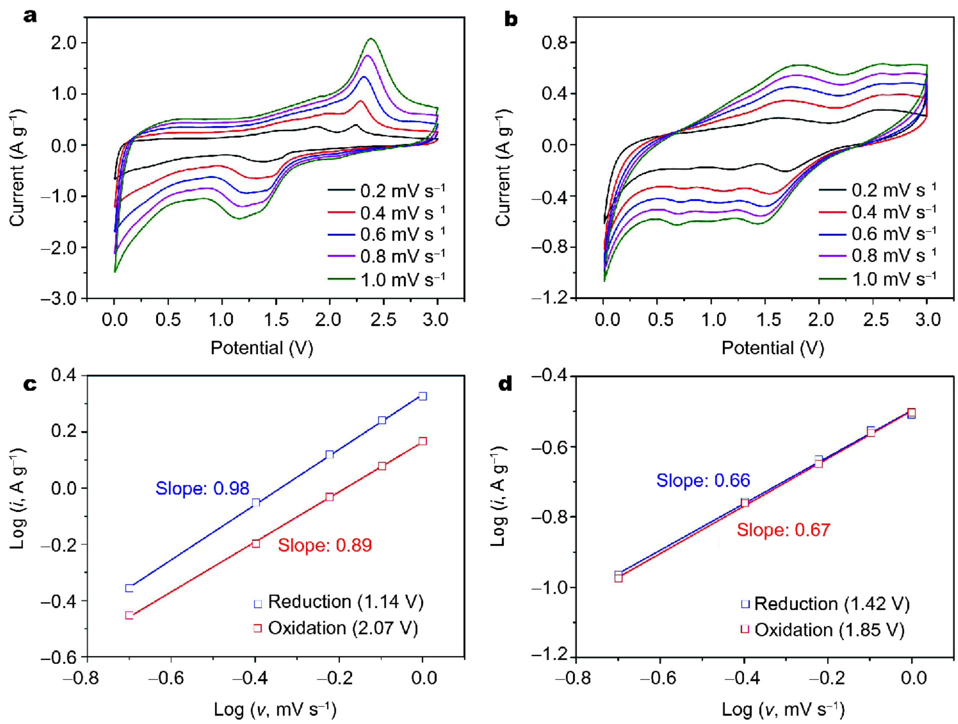

Figure 6 CV curves at 0.2–1.0 mV s^{-1} of (a) MoS_2/C nanospheres and (b) MoS_2/C floccules, (c, d) log *i vs.* log *v* plots for gaining obtaining *b*-values according to the above corresponding redox peaks.

reduction processes and 0.52 for the oxidation processes), indicating a rapid Li^+ storage process with a typical capacitive behavior for the MoS_2/C nanospheres. Moreover, they also exhibit a higher Li^+ diffusion coefficient compared to the MoS_2/C floccules (Fig. S5). As a consequence, the enhanced electrochemical behavior of the MoS_2/C nanospheres mainly results from the fast charge transfer and adequate electrolyte supply in MoS_2/C nanospheres during charge/discharge processes, thus achieving a high-rate capability.

The excellent lithium storage performance of the as-designed MoS_2/C nanospheres can be attributed to their unique structure. Specifically, the ultrathin MoS_2 nanosheets with broadened interlayer distance can greatly enrich the electrochemical active sites, leading to a high reversible specific capacity. Secondly, the vertical growth of MoS_2 nanosheets can provide direct electrons transfer path, avoiding the slow kinetics along *c*-axis direction of nanosheets. More impressively, designing sponge-like porous carbon core can be used not only as "reservoir" by adsorbing abundant electrolyte to shorten the ions-diffusion paths but also as a "elastomer" to buffer the structural change of the MoS_2 nanosheets during the charge/discharge processes. The direct evidence is the decreased charge transfer resistance and improved structural stability. Therefore, the as-obtained MoS_2/C nanospheres deliver a high rate capability and long cycle life.

CONCLUSIONS

In summary, we demonstrate the synthesis of ultrathin MoS_2 nanosheets *in-situ* grown on sponge-like carbon nanospheres by a simple diffusion-controlled process. The sponge-like carbon nanosphere core can adsorb and store abundant electrolyte for shortening the ions-diffusion path, and meanwhile plays as a "elastomer" for alleviating the structural change of the MoS_2 nanosheets during the charge/discharge processes. In addition, the vertical ultrathin MoS_2 nanosheets with enlarged interlayer distance from 0.62 to 0.89 nm also provide rich electrochemical active sites. Such facinating advantages render the as-obtained MoS_2/C nanospheres a high reversible capacity of 970 mA h g^{-1} at 0.1 A g^{-1}. The specific capacity is also well-maintained even after 100 cycles at 0.2 A g^{-1}. This design concept can be extended to exploit other high-performance electrode materials for advanced LIBs.

Received 7 December 2017; accepted 16 January 2018; published online 31 January 2018

1 Li W, Geng X, Guo Y, *et al.* Reduced graphene oxide electrically contacted graphene sensor for highly sensitive nitric oxide detection. ACS Nano, 2011, 5: 6955–6961
2 Deng Z, Jiang H, Hu Y, *et al.* 3D ordered macroporous MoS_2@C nanostructure for flexible Li-ion batteries. Adv Mater, 2017, 29: 1603020
3 Xie Y, Naguib M, Mochalin VN, *et al.* Role of surface structure on Li-ion energy storage capacity of two-dimensional transition-metal carbides. J Am Chem Soc, 2014, 136: 6385–6394
4 Deng D, Novoselov KS, Fu Q, *et al.* Catalysis with two-dimensional materials and their heterostructures. Nat Nanotechnol, 2016, 11: 218–230
5 Wang Z, Jia W, Jiang M, *et al.* Microwave-assisted synthesis of layer-by-layer ultra-large and thin NiAl-LDH/RGO nanocomposites and their excellent performance as electrodes. Sci China Mater, 2015, 58: 944–952
6 Wang Y, Yu L, Lou XWD. Synthesis of highly uniform molybdenum-glycerate spheres and their conversion into hierarchical MoS_2 hollow nanospheres for lithium-ion batteries. Angew Chem Int Ed, 2016, 55: 7423–7426
7 Zhang L, Wu HB, Yan Y, *et al.* Hierarchical MoS_2 microboxes constructed by nanosheets with enhanced electrochemical properties for lithium storage and water splitting. Energy Environ Sci, 2014, 7: 3302–3306
8 Shan TT, Xin S, You Y, *et al.* Combining nitrogen-doped graphene sheets and MoS_2: A unique film-foam-film structure for enhanced lithium storage. Angew Chem, 2016, 128: 12975–12980
9 Shi Y, Wang Y, Wong JI, *et al.* Self-assembly of hierarchical MoS_x/CNT nanocomposites (2<x<3): towards high performance anode materials for lithium ion batteries. Sci Rep, 2013, 3: 2169
10 Stephenson T, Li Z, Olsen B, *et al.* Lithium ion battery applications of molybdenum disulfide (MoS_2) nanocomposites. Energy Environ Sci, 2014, 7: 209–231
11 Zeng L, Pan A, Liang S, *et al.* Novel synthesis of V_2O_5 hollow microspheres for lithium ion batteries. Sci China Mater, 2016, 59: 567–573
12 Wang Z, Zhou L, David Lou XW. Metal oxide hollow nanostructures for lithium-ion batteries. Adv Mater, 2012, 24: 1903–1911
13 Yu XY, Yu L, Lou XWD. Metal sulfide hollow nanostructures for electrochemical energy storage. Adv Energy Mater, 2016, 6: 1501333
14 Niu C, Meng J, Han C, *et al.* VO_2 nanowires assembled into hollow microspheres for high-rate and long-life lithium batteries. Nano Lett, 2014, 14: 2873–2878
15 Pan AQ, Wu HB, Zhang L, *et al.* Uniform V_2O_5 nanosheet-assembled hollow microflowers with excellent lithium storage properties. Energy Environ Sci, 2013, 6: 1476
16 Wang Z, Luan D, Boey FYC, *et al.* Fast formation of SnO_2 nanoboxes with enhanced lithium storage capability. J Am Chem Soc, 2011, 133: 4738–4741
17 Wang B, Chen JS, Wu HB, *et al.* Quasiemulsion-templated formation of α-Fe_2O_3 hollow spheres with enhanced lithium storage properties. J Am Chem Soc, 2011, 133: 17146–17148
18 Wang J, Yang N, Tang H, *et al.* Accurate control of multishelled Co_3O_4 hollow microspheres as high-performance anode materials in lithium-ion batteries. Angew Chem, 2013, 125: 6545–6548
19 Xu S, Hessel CM, Ren H, *et al.* α-Fe_2O_3 multi-shelled hollow microspheres for lithium ion battery anodes with superior capacity and charge retention. Energy Environ Sci, 2014, 7: 632–637
20 Deng Z, Jiang H, Hu Y, *et al.* Nanospace-confined synthesis of coconut-like SnS/C nanospheres for high-rate and stable lithium-ion batteries. AIChE J, 2018, 529
21 Yang H, Su Y, Ding L, *et al.* Rational synthesis of SnS_2@C hollow microspheres with superior stability for lithium-ion batteries. Sci China Mater, 2017, 60: 955–962
22 An X, Yang H, Wang Y, *et al.* Hydrothermal synthesis of coherent porous V_2O_3/carbon nanocomposites for high-performance lithium- and sodium-ion batteries. Sci China Mater, 2017, 60: 717–727
23 Yu X, Hu H, Wang Y, *et al.* Ultrathin MoS_2 nanosheets supported on n-doped carbon nanoboxes with enhanced lithium storage and electrocatalytic properties. Angew Chem Int Ed, 2015, 54: 7395–7398
24 Li L, Li R, Gai S, *et al.* MnO_2 nanosheets grown on nitrogen-doped hollow carbon shells as a high-performance electrode for asymmetric supercapacitors. Chem Eur J, 2015, 21: 7119–7126
25 Sun Y, Hu X, Yu JC, *et al.* Morphosynthesis of a hierarchical MoO_2 nanoarchitecture as a binder-free anode for lithium-ion batteries. Energy Environ Sci, 2011, 4: 2870–2877
26 Zhang S, Yu X, Yu H, *et al.* Growth of ultrathin MoS_2 nanosheets with expanded spacing of (002) plane on carbon nanotubes for high-performance sodium-ion battery anodes. ACS Appl Mater Interfaces, 2014, 6: 21880–21885
27 Xie J, Zhang J, Li S, *et al.* Controllable disorder engineering in oxygen-incorporated MoS_2 ultrathin nanosheets for efficient hydrogen evolution. J Am Chem Soc, 2013, 135: 17881–17888
28 Hsiao MC, Chang CY, Niu LJ, *et al.* Ultrathin 1T-phase MoS_2 nanosheets decorated hollow carbon microspheres as highly efficient catalysts for solar energy harvesting and storage. J Power Sources, 2017, 345: 156–164
29 Xiong X, Luo W, Hu X, *et al.* Flexible membranes of MoS_2/C nanofibers by electrospinning as binder-free anodes for high-performance sodium-ion batteries. Sci Rep, 2015, 5: 9254
30 Wang PP, Sun H, Ji Y, *et al.* Three-dimensional assembly of single-layered MoS_2. Adv Mater, 2014, 26: 964–969
31 Zhou L, Zhang K, Sheng J, *et al.* Structural and chemical synergistic effect of CoS nanoparticles and porous carbon nanorods for high-performance sodium storage. Nano Energy, 2017, 35: 281–289
32 Lou P, Cui Z, Jia Z, *et al.* Monodispersed carbon-coated cubic NiP_2 nanoparticles anchored on carbon nanotubes as ultra-long-life anodes for reversible lithium storage. ACS Nano, 2017, 11: 3705–3715

Acknowledgements This work was supported by the National Natural Science Foundation of China (21522602, 51672082 and 91534202), the Shanghai Rising-Star Program (15QA1401200), the Innovation Program of Shanghai Municipal Education Commission, the Program for Professor of Special Appointment (Eastern Scholar) at Shanghai Institutions of Higher Learning, and the Fundamental Research Funds for the Central Universities (222201718002).

Author contributions Chen L, Jiang H and Li C conceived the idea and data analysis. Chen L performed the experiments. Hu Y and Wang H helped to discuss partial experimental data. Chen L and Jiang H wrote the paper. All authors contributed to the general discussion.

Conflict of interest The authors declare that they have no conflict of interest.

Supplementary information Supporting data are available in the online version of the paper.

Ling Chen is currently a PhD candidate in Materials and Science Engineering under the supervision of Prof. Hao Jiang at East China University of Science and Technology (ECUST). Her research centers on developing transition metal oxides/dichalcogenides for energy storage and conversion.

Hao Jiang received his PhD degree in Materials and Science Engineering from East China University of Science and Technology (ECUST), 2009. He then joined Temasek Laboratories, Nanyang Technological University (NTU) in Singapore, as a research scientist from 2009 to 2011. Now, he is a professor in Key Laboratory for Ultrafine Materials of Ministry of Education at ECUST. His research focuses on the design and synthesis of novel hierarchical nanomaterials for energy storage and conversion.

Chunzhong Li received BSc (1989), MSc (1992) and PhD (1997) from East China University of Science and Technology (ECUST). He became a full professor of School of Materials Science and Engineering in 1998, and now he is the dean of School of Materials Science and Engineering at ECUST. His research interests include functionalization and fabrication of nanomaterials for new energy, environment and relevant applications.

在多孔碳纳米球上原位生长超薄MoS_2纳米片构筑锂离子电池负极材料及其性能研究

陈灵, 江浩*, 胡彦杰, 王海燕, 李春忠*

摘要 开发具有快速充放电能力和长寿命的锂离子电池用电极材料是当前面临的巨大挑战. 本文中, 我们通过一个简单的扩散过程控制设计并合成了在多孔碳球上原位生长的超薄MoS_2纳米片. 这种类海绵状的多孔碳纳米球不仅可以吸附并储存大量的电解质, 有效地缩短了电化学反应过程中离子的传输路径; 而且还能用作类弹性体来缓冲表面活性电极材料在充放电过程中的结构变化. 此外, 这些超薄MoS_2纳米片的层间距扩大到0.89纳米, 极大地丰富了电化学活性位点. 因此, 与相应的MoS_2/C絮状物相比, 所制备的MoS_2/C纳米球表现出更高的比电容量和优异的循环稳定性. 我们希望这种设计理念可以延伸到其他高倍率、稳定电极材料的制备.

